

Unified description of scattering and fusion phenomena in heavy-ion collisions

Basudeb Sahu,¹ G. S. Mallick,² B. B. Sahu,¹ S. K. Agarwalla,³ and C. S. Shastri⁴

¹*Department of Physics, North Orissa University, Baripada 757003, India*

²*Department of Physics, Government College, Phulbani 764001, India*

³*Department of Applied Physics and Ballistics, Fakir Mohan University, Balasore 756019, India*

⁴*Department of Physics, Amrita Vishwa Vidyapeetham, Ettimadai, Coimbatore 641105, India*

(Received 23 July 2007; revised manuscript received 24 December 2007; published 11 February 2008)

An analytical recursive formula of the partial-wave scattering matrix for the total effective complex potential of nucleus-nucleus collisions is derived to conveniently analyze the data of angular variations of elastic scattering cross sections. Further, another expression of cross sections for the absorption from arbitrarily small intervals is derived. This leads to the explanation of the fusion cross section (σ_{fus}) data at various incident center-of-mass energies $E_{\text{c.m.}}$ by collecting the absorption contributions in the interior region of the effective potential. This concept is akin to that used by Udagawa *et al.* in the calculation of fusion cross sections in elastic channels. The interaction potential considered in the analysis is energy independent and by virtue of its weakly absorbing character it supports resonance states in different partial-wave trajectories. Consequently, occurrence of these resonances is shown to be the physical origin of the observed oscillatory structure in the variation respect to energy of the quantity $D(E_{\text{c.m.}}) = d^2(E_{\text{c.m.}}\sigma_{\text{fus}})/dE_{\text{c.m.}}^2$, the second derivative of the product $E_{\text{c.m.}}\sigma_{\text{fus}}$ with respect to $E_{\text{c.m.}}$. In this article, we investigate two well-known cases of heavy-ion collisions, namely $^{12}\text{C}+^{208}\text{Pb}$ and $^{16}\text{O}+^{208}\text{Pb}$, and obtain simultaneous and very successful explanations of cross sections for elastic scattering and fusion and the results of $D(E_{\text{c.m.}})$. These results obtained by using a somewhat novel and convenient method demonstrate the unified description of scattering and fusion for interacting heavy-ion systems.

DOI: [10.1103/PhysRevC.77.024604](https://doi.org/10.1103/PhysRevC.77.024604)

PACS number(s): 25.70.Bc, 24.10.-i, 25.70.Jj

I. INTRODUCTION

In the nucleus-nucleus collision process, there have been numerous experiments, and precise data of angular distribution of elastic scattering [$d\sigma(\theta)/d\sigma_R(\theta)$] at several incident energies and fusion cross sections [$\sigma_{\text{fus}}(E)$] at close energy intervals are available [1–5]. In this regard, we mention two such systems: $^{12}\text{C}+^{208}\text{Pb}$ in Refs. [1,3] and $^{16}\text{O}+^{208}\text{Pb}$ in Refs. [2,4], where these data are extensive. Unlike in light ion systems, the shape resonances generated by the effective potential in heavy-ion systems, though present, are hardly observable experimentally [6]. The possible influence and manifestation of such resonances in any other observable forms in the process of collision are to be investigated further. To analyze these data of heavy-ion collisions, one uses the phenomenological potential, which is usually complex. All the parameters describing the potential is set by fitting the measured data of elastic scattering cross section at various energies. Using the same interaction potential, one has to explain the fusion cross-section (σ_{fus}) data arising from the fusion process and resonance phenomena occurring via the elastic-scattering process of the colliding nuclei. In view of the fact that the scattering process is sensitive to the nature of the potential on the surface region and the fusion process is an interior activity, it is quite difficult to find a unique potential that can take care of both these phenomena simultaneously. Further, in the theoretical analysis, having obtained the elastic-scattering data, one can simply obtain the results of the total reaction cross section (σ_r), which includes the cross section for different reaction channels of which the fusion channel is predominant in the low-energy collision activities. Now, a problem arises in extracting the part of the

reaction cross section from the total σ_r , which can exactly account for the measured data of σ_{fus} .

Within the framework of optical potential model analysis of scattering, the expectation value of the imaginary part of the potential calculated using the distorted waves from the full potential in the elastic channel accounts for σ_r . This can simply be understood as and equated to the sum of the cross sections due to absorption in different regions of the potential where the imaginary part is actively present. Using the same wave function that describes the elastic-scattering data, one can obtain the absorption cross section σ_A^i in the infinitesimally small i th radial interval δr^i giving the total absorption cross section $\sigma_A = \sum_{i=1}^n \sigma_A^i$, where n is the total number of intervals such that the total range of the potential $R = \sum_{i=1}^n \delta r^i$. Using this expression, it becomes quite easy to give explicitly the amount of absorption over various regions or intervals of the potential. Based on the concept that fusion of two nuclei occurs in the region interior to the radial position (R_B) of the electrostatic Coulomb barrier, one expects that the absorption in this spatial region $0 < r < R_B$ has to account for the experimental data of fusion cross section ($\sigma_{\text{fus}}^{\text{expt}}$). The exact radius R_{fus} up to which the absorption cross section is to be calculated to explain $\sigma_{\text{fus}}^{\text{expt}}$ is known as the fusion radius. This concept of fusion cross section has been used in the direct reaction model (DRM) of Udagawa *et al.* [7,8]. However, they estimated the value of R_{fus} to be larger than the corresponding value of R_B in most of the heavy-ion systems analyzed, thereby theorizing that fusion initiates before crossing the Coulomb barrier. This is contrary to the popular assumption [9,10] that fusion takes place only after the barrier has been fully penetrated and hence this result has attracted severe criticism in the literature [11,12].

In our present calculation, we overcome this problem and explain results of $\sigma_{\text{fus}}^{\text{expt}}$ in the cases of $^{12}\text{C}+^{208}\text{Pb}$ and $^{16}\text{O}+^{208}\text{Pb}$ systems with the value of the R_{fus} parameter always less than the value of R_B in a given system.

We adopt a different method to solve the Schroedinger equation for a given nucleus-nucleus potential instead of using Runge-Kutta or similar methods of numerical integration. Our method is suitable for the study of regionwise absorption in the reaction process. In our calculation, we simulate the potential by arbitrarily small rectangular parts and, using exact wave functions and their analytical continuation in between neighboring parts, we obtain analytical expression for the scattering matrix (S -matrix) that is used to explain the elastic-scattering data. Using the same wave functions, the amount of absorption in each small part (width) of the potential is calculated. The sum of contributions for absorption of all the parts covering the whole range of the potential is found to be equal to the total reaction cross section σ_r . However, to account for the value of fusion cross section σ_{fus} , which is always less than that of σ_r , we consider the sum of the contributions for absorption over a limited region $0 < r < R_{\text{fus}}$ within the radial position R_B of the Coulomb barrier. We have verified that the results of elastic scattering obtained by our procedure and Runge-Kutta method are same.

Measurements with high precision provide results of σ_{fus} at very close energy intervals in the collision of two heavy nuclei at incident energies near the Coulomb barrier. The variation of the results of σ_{fus} with bombarding center-of-mass energy $E_{\text{c.m.}}$ looks smoothly varying without any special feature or structure in the cases of heavy pairs of nuclei, though it is oscillatory in light colliding pairs. But, when the product $E_{\text{c.m.}}\sigma_{\text{fus}}$ is differentiated twice with respect to $E_{\text{c.m.}}$ using some point difference formula, the corresponding result of $D(E_{\text{c.m.}}) = d^2(E_{\text{c.m.}}\sigma_{\text{fus}})/dE_{\text{c.m.}}^2$, generally referred to as the barrier distribution, exhibits peculiar oscillatory structure in its variation with $E_{\text{c.m.}}$ [5]. The theoretical results of σ_{fus} obtained in our above method of regionwise absorption at various incident $E_{\text{c.m.}}$ is presented in the form of $D(E_{\text{c.m.}})$ and the corresponding experimental results of $D(E_{\text{c.m.}})$ in the cases of $^{12}\text{C}+^{208}\text{Pb}$ [3] and $^{16}\text{O}+^{208}\text{Pb}$ [4] systems are explained with remarkable success, addressing the peak structure in detail. In this analysis, we find the following important characteristics in the potential used by us: (i) the real part is very deep and has small diffuseness and (ii) the imaginary part is comparatively weak. As a result of this less absorptive nature of the potential, shape resonance states (experimentally unobserved) [6] could survive in the collision process due to the formation of standing waves in the nuclear well. As a consequence, these resonances become responsible for the oscillatory structure in the results of $D(E_{\text{c.m.}})$ as a function of $E_{\text{c.m.}}$.

It may be mentioned here that the natural language for studying fusion reactions at energy around the Coulomb barrier is the coupled-channels (CC) formulation. Various computer codes such as CCFUS [13,14] and CCFULL [15] are developed for this purpose. Due to the complex nature of the heavy-ion collision process, the number of channels encountered is very large and the solution of coupled equations incorporating all these channels becomes very complicated and tedious. Such formulations are, however, somewhat schematic

and include important approximations to ease the process of calculations. It has been observed [4] that simultaneous explanation of the shapes of both σ_{fus} and $D(E_{\text{c.m.}})$ in most pairs of nuclei is far from satisfactory no matter how exhaustive the CC calculation is. This disappointing situation still persists in the recent CC calculations [16] based on M3Y plus repulsion potential applied to the analysis of the data of the $^{16}\text{O}+^{208}\text{Pb}$ system. In a most recent calculation [17], it is reported that even the measured data of σ_{fus} alone from deep sub-barrier region to the above barrier region of energy cannot be reproduced simultaneously by the CC calculations with same Woods-Saxon nuclear potential. The microscopic CC calculation is basically a one-dimensional barrier passing model [18,19] incorporating a large number of barriers of different heights generated due to coupling between the relative motion and the internal degrees of freedom of the colliding nuclei such as static deformation, collective vibration [20], inelastic excitation, and nucleon transfer [16]. Thus, the CC calculation for fusion cross section does not incorporate the effect of any mechanism generated by the interaction potential in the interior pocket region, which is considered highly absorptive to impose ingoing-wave boundary condition for the barrier-passing model.

In the present formulation, the nucleus-nucleus potential in the interior or pocket region plays an important role in accounting for the experimental results of σ_{fus} and the corresponding function $D(E_{\text{c.m.}})$ derived from measured σ_{fus} . The resonances generated by the pocket due to its less absorptive nature describe the the oscillatory structure of $D(E_{\text{c.m.}})$ with remarkable success. Further, the effect of coupling is invoked, though not explicitly, in our formulation as follows. The coupling of a nonelastic channel with the entrance channel is expected to change the shape of the entrance channel potential barrier significantly [21], particularly in the interior region $r < R_B$ such that there is a sharp fall in the effective potential in the inner region [22,23]. This effect of coupling can be readily incorporated in the formulation by using a small value for the diffuseness parameter in the Woods-Saxon form of nuclear potential. The present formulation uses such small diffuseness parameter in the simultaneous analysis of elastic scattering and fusion cross-section data and, hence, incorporates the effect of channel coupling in a phenomenological way.

In Sec. II, we present the formulation for analytical expression for S -matrix and regionwise absorption. Application of the formulation is done in Sec. III to the analysis of experimental data of $d\sigma(\theta)/d\sigma_R(\theta)$, $\sigma_{\text{fus}}(E_{\text{c.m.}})$, and $D(E_{\text{c.m.}})$ in the cases of $^{12}\text{C}+^{208}\text{Pb}$ and $^{16}\text{O}+^{208}\text{Pb}$ systems. We summarize the results in Sec. IV.

II. FORMULATION

The solution of the radial Schroedinger equation for a complex Coulomb nuclear potential is the most important part of scattering and reaction cross section in the nuclear optical model widely used in the study of heavy-ion collision. The effective potential in the radial equation is a sum of the complex nuclear potential [$V_N(r)$], the electrostatic or Coulomb potential [$V_C(r)$], and the centrifugal term [$V_\ell(r)$].

Use of the Runge-Kutta- (RK) type method of numerical integration is most popular in solving the Schroedinger equation with this potential to get the wave function and its derivative at a radial point outside the range of the nuclear potential that is then connected to the corresponding exact Coulomb wave function and its derivative to obtain the results of the scattering matrix for the analysis of scattering data and so on. But the extraction of a part of the reaction cross section from the total reaction cross section to analyze the fusion cross section is not straightforward in this method. Hence, in this article we adopt a convenient but somewhat different procedure to solve the Schroedinger equation.

Let us first consider the s -wave scattering in detail. A potential $U(r)$ can be considered as a chain of n number of rectangular potentials, each of which has arbitrarily small width w . In fact in any numerical integration of differential equation similar procedure is implicit. Having simulated the potential up to a maximum range of $r = R_{\max}$, we have $R_{\max} = \sum_i^n w_i$, where $w_i = w$ is the width of the i th rectangle.

Let, in the j th region, $\sum_{i=1}^{j-1} w_i < r \leq \sum_{i=1}^j w_i$, the strength and width of the potential are denoted by U_j and w_j , respectively. The reduced Schroedinger equation in this region is

$$\frac{d^2\Phi(r)}{dr^2} + \frac{2m}{\hbar^2}(E - U_j)\Phi(r) = 0, \quad (1)$$

with the following solution

$$\Phi_j(r) = a_j e^{ik_j r} + b_j e^{-ik_j r}, \quad (2)$$

where the wave number k_j is defined as $k_j = \sqrt{\frac{2m}{\hbar^2}(E - U_j)}$ for the j th segment of width w_j . For two adjacent segments, we use the notation $q_{ji} = -q_{ij} = k_j - k_i/k_j + k_i$. Here, E indicates the incident energy and m stands for the mass of the particle. Explicitly, the solution in first three segments close to the origin $r = 0$ can be written as

$$\Phi_I = \sin k_1(r - c_1), \quad 0 < r < w_1 \quad (3)$$

$$\Phi_{II} = a_2 e^{ik_2(r-c_2)} + b_2 e^{-ik_2(r-c_2)}, \quad w_1 < r < (w_1 + w_2) \quad (4)$$

$$\Phi_{III} = a_3 e^{ik_3(r-c_3)} + b_3 e^{-ik_3(r-c_3)}, \quad (w_1 + w_2) < r < (w_1 + w_2 + w_3) \quad (5)$$

Here, a_2 , b_2 , a_3 , and b_3 stand for the coefficients of the wave functions and c_1 , c_2 , and c_3 indicate some arbitrary constants.

Matching the wave functions and the derivatives at the boundary at $r = w_1$, we get

$$a_2 = \frac{1}{2} e^{-ik_2(w_1-c_2)} \left[\sin k_1(w_1 - c_1) + \frac{k_1}{ik_2} \cos k_1(w_1 - c_1) \right], \quad (6)$$

$$b_2 = \frac{1}{2} e^{ik_2(w_1-c_2)} \left[\sin k_1(w_1 - c_1) - \frac{k_1}{ik_2} \cos k_1(w_1 - c_1) \right], \quad (7)$$

$$\frac{a_2}{b_2} = e^{-2ik_2(w_1-c_2)} \times q_{21}, \quad (8)$$

where

$$q_{21} = \frac{\sin k_1(w_1 - c_1) + \frac{k_1}{ik_2} \cos k_1(w_1 - c_1)}{\sin k_1(w_1 - c_1) - \frac{k_1}{ik_2} \cos k_1(w_1 - c_1)}. \quad (9)$$

Similar calculation at the boundary at $r = w_1 + w_2$ yields

$$a_3 = \frac{1}{2} e^{-ik_3(w_1+w_2-c_3)} b_2 e^{-ik_2(w_1+w_2-c_3)} \times \left[\left(1 - \frac{k_2}{k_3}\right) + \left(1 + \frac{k_2}{k_3}\right) e^{2ik_2 w_2} q_{21} \right], \quad (10)$$

$$b_3 = \frac{1}{2} e^{ik_3(w_1+w_2-c_3)} b_2 e^{-ik_2(w_1+w_2-c_3)} \times \left[\left(1 + \frac{k_2}{k_3}\right) + \left(1 - \frac{k_2}{k_3}\right) e^{2ik_2 w_2} q_{21} \right], \quad (11)$$

$$\frac{a_3}{b_3} = e^{-2ik_3(w_1+w_2-c_3)} \times q_{321}, \quad (12)$$

where

$$q_{321} = \frac{q_{32} + q_{21} e^{2ik_2 w_2}}{1 + q_{32} \times q_{21} e^{2ik_2 w_2}} \quad (13)$$

and

$$q_{32} = \frac{k_3 - k_2}{k_3 + k_2}. \quad (14)$$

This can be generalized for n boundaries to give

$$\frac{a_n}{b_n} = e^{-2ik_n \left(\sum_{j=1}^{n-1} w_j - c_n\right)} \times q_{n,n-1,n-2,\dots,1}, \quad (15)$$

$$q_{n,n-1,n-2,\dots,1} = \frac{q_{n,n-1} + q_{n-1,n-2,\dots,1} e^{2ik_{n-1} w_{n-1}}}{1 + q_{n,n-1} \times q_{n-1,n-2,\dots,1} e^{2ik_{n-1} w_{n-1}}}, \quad (16)$$

\vdots

$$q_{21} = \frac{\sin k_1(w_1 - c_1) + \frac{k_1}{ik_2} \cos k_1(w_1 - c_1)}{\sin k_1(w_1 - c_1) - \frac{k_1}{ik_2} \cos k_1(w_1 - c_1)}, \quad (17)$$

where $q_{n,n-1} = k_n - k_{n-1}/k_n + k_{n-1}$.

Setting the arbitrary constants as $c_1 = w_1$ and

$$c_n = \sum_{j=1}^{n-1} w_j,$$

we get

$$D^{(0)} = \frac{a_n}{b_n} = q_{n,n-1,n-2,\dots,1} = \frac{q_{n,n-1} + q_{n-1,n-2,\dots,1} e^{2ik_{n-1} w_{n-1}}}{1 + q_{n,n-1} \times q_{n-1,n-2,\dots,1} e^{2ik_{n-1} w_{n-1}}}, \quad (18)$$

with

$$q_{n-1,n-2,\dots,1} = \frac{q_{n-1,n-2} + q_{n-2,n-3,\dots,1} e^{2ik_{n-2} w_{n-2}}}{1 + q_{n-1,n-2} \times q_{n-2,n-3,\dots,1} e^{2ik_{n-2} w_{n-2}}}, \quad (19)$$

\vdots

$$q_{21} = -1. \quad (20)$$

Using the recursive character of the formula for $q_{n,n-1,n-2,\dots,1}$, the function in the m region can be expressed in terms of that in the $(m - 1)$ region. With this we can develop a straightforward

numerical program for the n -step potential for the evaluation of the scattering matrix and the wave function at a given incident energy, having simulated the potential $U(r)$ by n -step potentials. If $\sum_{i=1}^n w_i = R_n = R_{\max}$, such that the potential $U_j(r)$ considered in Eq. (1) is zero for $r > R_n$, it can be easily understood that the s -wave S -matrix is given by $S_0 = -\frac{a_n}{b_n}$ and the total absorption or reaction cross section in the region $0 < r < R_n$ is given by

$$\sigma_{\text{abs}}^{(0)} = \frac{\pi}{k^2} \left(1 - \frac{|a_n|^2}{|b_n|^2} \right).$$

Similarly, $S_0^p = -\frac{a_p}{b_p}$ can be interpreted as the S -matrix of the original potential truncated at $R_p (= \sum_{i=1}^p w_i) < R_{\max}$. Hence, $\frac{\pi}{k^2} (1 - \frac{|a_p|^2}{|b_p|^2})$ can be taken as the absorption cross section generated in the region $0 < r < R_p$. Thus, $\frac{\pi}{k^2} [(1 - \frac{|a_p|^2}{|b_p|^2}) - (1 - \frac{|a_q|^2}{|b_q|^2})]$ shall give the contribution to the absorption cross section from the region $R_p > r > R_q = \sum_{i=1}^q w_i$.

Taking the complex conjugate of the Schrodinger equation (1) and rearranging, we get

$$2ik_n(|a_n|^2 - |b_n|^2) = \int_0^{R_n} 2i \text{Im} U(r) \Phi \Phi^* dr, \quad (21)$$

$$1 - \frac{|a_n|^2}{|b_n|^2} = I_1 + I_2 + \dots, \quad (22)$$

$$I_1 = -\frac{1}{k_n} \int_0^{w_1} \text{Im} U(r) \left| \frac{\Phi}{b_n} \right|^2 dr, \quad (23)$$

$$I_2 = -\frac{1}{k_n} \int_{w_1}^{(w_1+w_2)} \text{Im} U(r) \left| \frac{\Phi}{b_n} \right|^2 dr. \quad (24)$$

Using the respective wave function and the potential in a given segment, we simplify the corresponding integral and obtain

$$I_1 = \left(-\frac{1}{k_n} \right) \frac{\text{Im} U_1}{|b_n|^2} \left\{ \frac{|b_1|^2}{2\text{Im} k_1} (e^{2\text{Im} k_1 w_1} - 1) - \frac{|b_1|^2}{2\text{Im} k_1} (e^{-2\text{Im} k_1 w_1} - 1) + \frac{1}{\text{Re} k_1} \text{Im} [a_1 b_1^* (e^{2i \text{Re} k_1 w_1} - 1)] \right\}, \quad (25)$$

$$I_2 = \left(-\frac{1}{k_n} \right) \frac{\text{Im} U_2}{|b_n|^2} \left\{ \frac{|b_2|^2}{2\text{Im} k_2} e^{-2\text{Im} k_2 w_1} (e^{2\text{Im} k_2 w_2} - 1) - \frac{|b_2|^2}{2\text{Im} k_2} e^{2\text{Im} k_2 w_1} (e^{-2\text{Im} k_2 w_2} - 1) + \frac{1}{\text{Re} k_2} \text{Im} [a_2 b_2^* e^{2\text{Im} k_2 w_1} (e^{2i \text{Re} k_2 w_2} - 1)] \right\}. \quad (26)$$

This result in the j th segment can be expressed as

$$I_j = \left(-\frac{1}{k_n} \right) \frac{\text{Im} U_j}{|b_n|^2} \left\{ \frac{|b_j|^2}{2\text{Im} k_j} e^{-2\text{Im} k_j w_{j-1}} (e^{2\text{Im} k_j w_j} - 1) - \frac{|b_j|^2}{2\text{Im} k_j} e^{2\text{Im} k_j w_{j-1}} (e^{-2\text{Im} k_j w_j} - 1) + \frac{1}{\text{Re} k_j} \text{Im} [a_j b_j^* e^{2\text{Im} k_j w_{j-1}} (e^{2i \text{Re} k_j w_j} - 1)] \right\}. \quad (27)$$

The asterisk indicates the complex conjugate of the respective quantity. So that

$$1 - \frac{|a_n|^2}{|b_n|^2} = \sum_{j=1}^n I_j, \quad (28)$$

with

$$R_n = \sum_{j=1}^n w_j = R_{\max}. \quad (29)$$

Considering same width for all segments, i.e., $w = w_1 = w_2 = w_3 = \dots$, we have $n = \frac{R_{\max}}{w}$.

The procedure for calculation of S -matrix through Eqs. (18)–(20) with a multistep potential (MP) approximation makes the procedure an algebraic recursive method that can be easily programmed. The Eqs. (27)–(29) give a method to study the absorption cross section as discrete sums of contributions from various sections.

Generalization of this procedure for the complex heavy-ion Coulomb nuclear problem for all partial waves is straightforward. The problem of higher partial waves can be treated as the scattering by the effective potential $V_N(r) + V_C(r) + V_\ell(r)$ and one can adopt the MP approximation method described above for this effective potential. In the complex potential scattering, the subtlety involved regarding the $r^{\ell+1}$ behavior of the wave function very close to the origin is not very critical for the following reasons. In the case of complex absorptive potential, the suitably normalized wave function in general rapidly attenuates to zero well beyond origin because of the presence of absorption. Hence, one can start the calculation of the S -matrix well beyond $r = 0$, where the multistep approximation is quite accurate. We have verified that the results of the S -matrix and cross sections obtained by our procedure are essentially the same as those obtained by conventional methods.

In the region $0 < r \leq R_{\max}$, the potential consists of all the three parts, $V_N(r)$, $V_C(r)$, and $V_\ell(r)$. But in the outer region $r \geq R_{\max}$, the potential of the nucleus-nucleus interaction is only Coulombic [$V_C(r)$] with the centrifugal terms $V_\ell(r) = \frac{\hbar^2 \ell(\ell+1)}{2m r^2}$ for different angular momentum partial wave ℓ .

Using the exact Coulomb wave functions, i.e., G_ℓ and F_ℓ and their derivatives G'_ℓ and F'_ℓ , in the outer region $r \geq R_{\max}$ and the wave function $\Phi_n(r) = a_n e^{ik_n r} + b_n e^{-ik_n r}$ and its derivative $\Phi'_n(r)$ in the left side of $r = R_{\max}$, and matching them at $r = R_{\max}$, we get the expression for partial wave S -matrix η_ℓ as

$$\eta_\ell = 2i C_\ell + 1, \quad (30)$$

where

$$C_\ell = \frac{k F'_\ell - F_\ell H}{H(G_\ell + i F_\ell) - k(G'_\ell + i F'_\ell)}, \quad (31)$$

$$H = \frac{\Phi'_n}{\Phi_n} = ik_n \frac{D^{(\ell)} e^{ik_n R_{\max}} - e^{-ik_n R_{\max}}}{D^{(\ell)} e^{ik_n R_{\max}} + e^{-ik_n R_{\max}}}, \quad (32)$$

$$D^{(\ell)} = \frac{a_n}{b_n}, \quad (33)$$

with $k_n = \sqrt{\frac{2m}{\hbar^2}(E - V_n)}$, which is real at $r = R_{\max}$, where the potential $V_n = V_C + V_\ell$ is real and $E > V_n$.

Using the above expression (30) for η_ℓ , we explain the elastic scattering of a given system. For the total reaction cross section one can use the formula

$$\sigma_r = \frac{\pi}{k^2} \sum_\ell (2\ell + 1)(1 - |\eta_\ell|^2). \quad (34)$$

As formulated above, this is equal to the absorption cross section

$$\begin{aligned} \sigma_{\text{abs}} &= \frac{\pi}{k^2} \sum_\ell (2\ell + 1) \left(1 - \frac{|a_n|^2}{|b_n|^2} \right) \\ &= \frac{\pi}{k^2} \sum_\ell (2\ell + 1) \left[\sum_{j=1}^n I_j^{(\ell)} \right]. \end{aligned} \quad (35)$$

The contribution to absorption or reaction cross section from any part within the range $0 - R_{\max}$ can be obtained by considering the corresponding number of segments in the above summation. This is the unambiguous calculation of regionwise absorption in the collision process with no disturbance of potential and hence the wave function that explain the angular distribution of elastic-scattering data. If one wishes to obtain the amount of absorption cross section in the region $0 < r < R_{\text{fus}}$, where $R_{\text{fus}} < R_{\max}$, the total number of segments to be considered in the summation (35) is $n_{\text{fus}} = \frac{R_{\text{fus}}}{w}$. The resulting cross section

$$\sigma_{\text{fus}} = \frac{\pi}{k^2} \sum_\ell (2\ell + 1) \left[\sum_{j=1}^{n_{\text{fus}}} I_j^{(\ell)} \right] \quad (36)$$

corresponds to the fusion cross section in the framework of the DRM [7], as discussed in the Introduction.

At this stage a brief discussion of this MP formulation as a numerical method is desirable. This approach is in a way the simplest approximation to the solution of the differential equation as compared to the trapezoidal rule using straight-line sections, Simpson's rule using parabolic sections, and the spline method using cubic polynomials [24–26]. The latter methods are very useful for a more precise calculation of the wave function but have the disadvantage of not being amenable to simple algebraic representations in different intervals. However, in the nuclear cross-section calculation, considering the experimental errors involved, the calculation of the wave function and the cross section up to three to four significant places of decimal is quite adequate. We have compared the numerical results obtained by using the MP method in one dimension with that of RK and exact solution for typical potentials like Eckart and Ginocchio potentials in a recent article [27] and found that results agree up to three significant places. As described in this section, our analytical formulation leads to a neat recursive relation facilitating the calculation of the S -matrix and cross sections. In particular, estimation of contribution to absorption in different segments of the potential and study of the nature of the wave function and its normalization can be carried out in a transparent way in this MP formulation. However, in the nucleus-nucleus optical

model calculations carried out using standard procedures like the RK method [28], because of the imaginary potential, the wave function rises rapidly and hence needs to be appropriately renormalized at several stages to carry out the efficient phase-shift calculations. This makes the estimation of regionwise contributions to the cross section and reactions more cumbersome [29]. To demonstrate the feasibility and applicability of this MP method in nuclear-scattering analysis, in this article we carried out the calculations of cross sections of both elastic scattering and fusion in heavy-ion collisions and compared them with the respective experimental results with remarkable success. The numerical results of elastic-scattering cross sections presented in this article are also verified using standard optical model methods [28].

III. APPLICATION

We applied the formulation developed in Sec. II to the analysis of the collision data of two typical heavy-ion systems, namely $^{12}\text{C} + ^{208}\text{Pb}$ and $^{16}\text{O} + ^{208}\text{Pb}$, and obtained a unified and consistent description of the measured cross sections of elastic scattering and fusion and the peculiar peak structure in the variation of the quantity $D(E_{\text{c.m.}}) = \frac{d^2(E_{\text{c.m.}}\sigma_{\text{fus}})}{dE_{\text{c.m.}}^2}$ as a function of $E_{\text{c.m.}}$.

In the optical model potential (OMP) analysis of scattering of two nuclei of mass number A_1 and A_2 and proton numbers Z_1 and Z_2 , the OMP is described by

$$V(r) = -V_N f(r, R_V, a_V) - iWg(r, R_W, a_W) + V_C(r)$$

in the entrance channel. The form factor used in this article is

$$f(r, R, a) = g(r, R, a) = [1 + \exp\{(r - R)/a\}]^{-1}.$$

V_N and W are the strength of real and imaginary parts of OMP. The radius parameters are expressed as $r_V = R_V/(A_1^{1/3} + A_2^{1/3})$ and $r_W = R_W/(A_1^{1/3} + A_2^{1/3})$. The symbols a_V and a_W indicate diffuseness parameters. The Coulomb potential $V_C(r)$ is given by

$$V_C(r) = \frac{Z_1 Z_2 e^2 (3 - r^2/R_C^2)}{2R_C}, \quad r \leq R_C;$$

$$V_C(r) = Z_1 Z_2 e^2 / r, \quad r > R_C,$$

where $R_C = r_C(A_1^{1/3} + A_2^{1/3})$ with r_C as the Coulomb radius parameter. Thus, there are a total of seven parameters, $V_N, r_V, a_V, W, r_W, a_W$, and r_C , in this OMP.

A. Elastic-scattering cross section

We know that there can be several sets of parameters describing the potential that can explain the angular distribution of elastic scattering equally well. In our present calculation, all seven parameters are energy independent and while selecting the values of the parameters for the potential we are motivated by the fact that resonance can be manifested if the imaginary part W is weak and, further, such a weak absorption is sufficient if the real part is considered deep [30] and less diffused [31] to explain the elastic-scattering cross section. In Table I, the

TABLE I. Optical model potential parameters used in the calculations. V_B and R_B represent height and radial position of the Coulomb barrier, respectively.

System	V_N (MeV)	r_V (fm)	a_V (fm)	W (MeV)	r_W (fm)	a_W (fm)	r_C (fm)	V_B (MeV)	R_B (fm)	R_{fus} (fm)
$^{12}\text{C}+^{208}\text{Pb}$	125	1.31	0.320	3.0	1.325	0.25	0.90	56.7	12.16	9.9
$^{16}\text{O}+^{208}\text{Pb}$	125	1.35	0.285	2.0	1.320	0.15	1.02	73.7	12.52	8.8

values of the OMP parameters used in the calculation for the analysis of elastic scattering data for the $^{12}\text{C}+^{208}\text{Pb}$ and $^{16}\text{O}+^{208}\text{Pb}$ systems are given. Table I also contains the values of height V_B and radius R_B of the s -wave barrier for each of the above two systems.

In the case of $^{12}\text{C}+^{208}\text{Pb}$, as per the above prescription, the real part is made deep with depth $V_N = 125$ MeV and less diffused with diffuseness parameter $a_V = 0.32$ fm along with the radius parameter $r_V = 1.31$ fm. The imaginary part is given a weak attractive strength $W = 3.0$ MeV along with other parameters $r_W = 1.325$ fm and $a_W = 0.25$ fm. The value of the Coulomb radius parameter is taken to be $r_C = 0.9$ fm. For a pictorial view, the real part of the combined nuclear and Coulomb potentials for s -wave can be plotted as a function of radial distance in Fig. 1. This clearly shows a repulsive barrier falling sharply in the interior side with height $V_B = 56.7$ MeV and position $R_B = 12.16$ fm as mentioned in Table I for the $^{12}\text{C}+^{208}\text{Pb}$ system. As pointed out in the formulation the potential is simulated by n number of rectangular potentials, each of width equal to 0.008 fm in the spatial region $0 < r \leq R_{\max}$. The region $r > R_{\max} \approx 15$ fm is the region where the nuclear potential along with its imaginary part is zero leaving the effective potential only as Coulombic with the centrifugal term. Using the S -matrix given by the expression (30), we obtain the results of angular variation of differential scattering cross section at laboratory energies 58.9,

60.9, 62.9, 64.9, 74.9, and 84.9 MeV. These calculated results are represented by solid curves in Fig. 2 and they are compared with the corresponding experimental data taken from Ref. [1] and shown by solid dots in the same figure. It is clearly seen that the explanation of the data in each case of energy is quite good. It may be pointed out here that to explain the data for all energies from 58.9 to 84.9 MeV, we have used the same set of OMP parameters given in Table I. In other words, the values of OMP parameters are energy independent. We may mention further that the value of $r_C = 0.9$ fm considered here is a bit lower than the usual value $r_C = 1.25$ fm. We have seen that it does not affect the results of the elastic-scattering cross section in our calculation and this fact is corroborated by the finding of the calculation in Ref. [32] with regard to Coulomb potentials in heavy-ion interactions. To maintain consistency, we have used this smaller value of r_C to account for the fusion cross-section data at low energy for this $^{12}\text{C}+^{208}\text{Pb}$ system that will be discussed below.

Similar calculations are done for the $^{16}\text{O}+^{208}\text{Pb}$ system. In this case also, we have considered a deep real potential with depth $V_N = 125$ MeV and small diffuseness parameter $a_V = 0.285$ fm. Values of other parameters are given in Table I. The plot of the real part of nuclear plus Coulomb potentials as a function of radial distance for the s -wave in Fig. 3 shows a barrier falling sharply in the interior side with height $V_B = 73.7$ MeV and radius $R_B = 12.52$ fm for

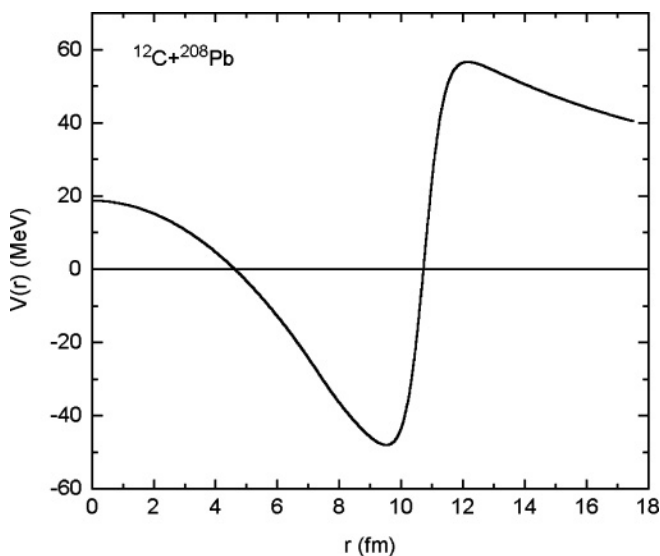


FIG. 1. Plot of real part of nuclear plus Coulomb potentials for partial wave $\ell = 0$ as a function of radial distance with potential parameters $V_0 = -125$ MeV, $r_V = 1.31$ fm, $a_V = 0.32$ fm, and $r_C = 0.9$ fm for the $^{12}\text{C}+^{208}\text{Pb}$ system.

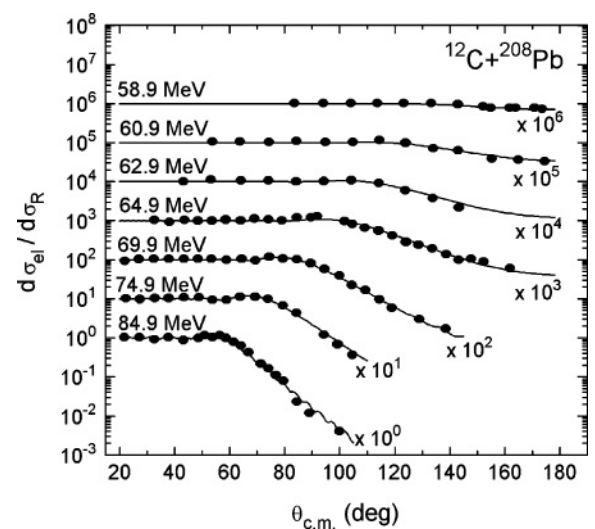


FIG. 2. Angular distribution of elastic-scattering cross sections (ratios to Rutherford) of $^{12}\text{C}+^{208}\text{Pb}$ system at laboratory energies 58.9, 60.9, 62.9, 64.9, 69.9, 74.9, and 84.9 MeV. The full drawn curves are theoretical results of the present optical model calculation. The circles are experimental cross sections from Ref. [1].

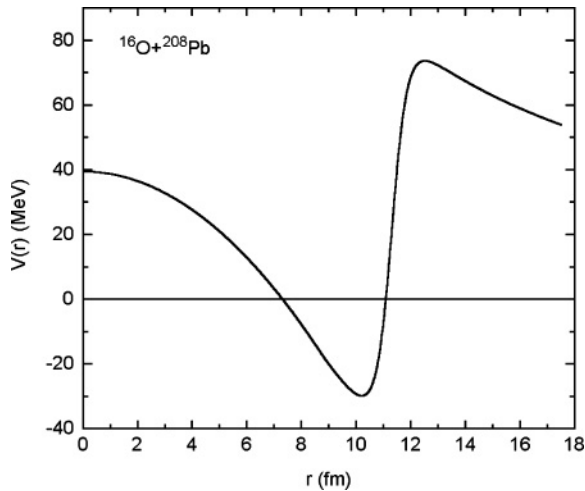


FIG. 3. Plot of real part of nuclear plus Coulomb potentials for partial wave $\ell = 0$ as a function of radial distance with potential parameters $V_0 = -125$ MeV, $r_V = 1.339$ fm, $a_V = 0.285$ fm, and $r_C = 1.02$ fm for the $^{16}\text{O}+^{208}\text{Pb}$ system.

this system. In Fig. 4, we compare our calculated results (solid curves) of differential scattering cross section with the corresponding experimental data (solid dots) taken from Ref. [2] at several laboratory energies, 80, 83, 88, 90, 96, and 102 MeV. It is clearly seen that the explanation of the data for all energies is good. Here also we have used a single potential for all energies and a smaller value $r_C = 1.02$ fm. The finding of such energy-independent OMP is an important outcome of this analysis in view of the requirement that such potential is crucial in the description of fusion data to be carried out below for the above two systems.

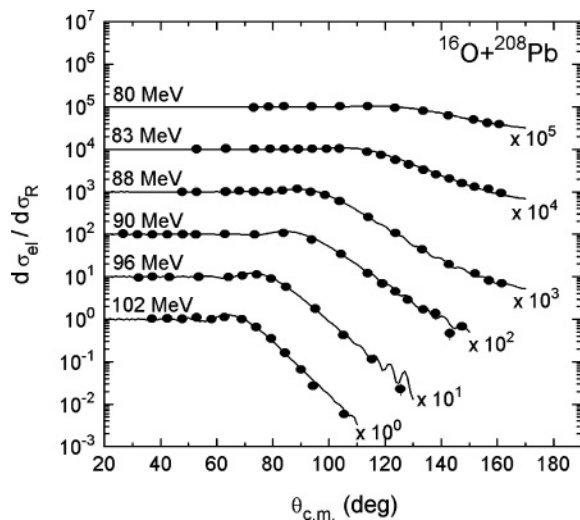


FIG. 4. Same as Fig. 2 for $^{16}\text{O}+^{208}\text{Pb}$ system at laboratory energies 80, 83, 88, 90, 96, and 102 MeV. The full drawn curves are theoretical results of the present optical model calculation. The circles are experimental cross sections from Ref. [2].

B. Fusion cross section

In the low-energy collision process, fusion of the two nuclei is another important process actively associated with the elastic-scattering event. In the simultaneous estimate of cross sections for elastic scattering and fusion, it is trivial to consider that fusion cross section σ_{fus} is a part of total reaction cross section σ_r . But it is always a Herculean task to extract the part from σ_r to exactly account for the measured results of σ_{fus} at various incident energies over a wide range. We consider here the DRM of Udagawa *et al.* [7] to calculate σ_{fus} . In this model, the fusion cross section is defined as the amount of absorption cross section within the interior region $0 < r < R_{\text{fus}}$, where R_{fus} is a radial distance expected to be less than R_B , which is the radial position of the s -wave Coulomb barrier in the case of a given nucleus-nucleus system. In the formulation through Eq. (36), we calculated the values of σ_{fus} as per the above principle of the DRM. The results are shown in Figs. 5(a), 5(b), 6(a), and 6(b). Discussion of Figs. 5(b) and 6(b) is done in the next subsection.

Using $R_{\text{fus}} = 9.9$ fm, we obtain the results of σ_{fus} for the $^{12}\text{C}+^{208}\text{Pb}$ system and compare it (solid curve) in Fig. 5(a) with the corresponding experimental data (solid dots) taken from Ref. [3]. It is clearly seen that the matching of the data over the whole range of energy from $E_{\text{c.m.}} = 50$ to 75 MeV is quite good. In achieving this fitting we have not changed the values of the parameters of the OMP that explain the elastic-scattering data in Fig. 2. As demanded by the acceptable physical situation, the value of $R_{\text{fus}} = 9.9$ fm used in our calculation is less than the value of Coulomb radius $R_B = 12.16$ fm in this system. Further, the importance of the present successful description of elastic scattering and

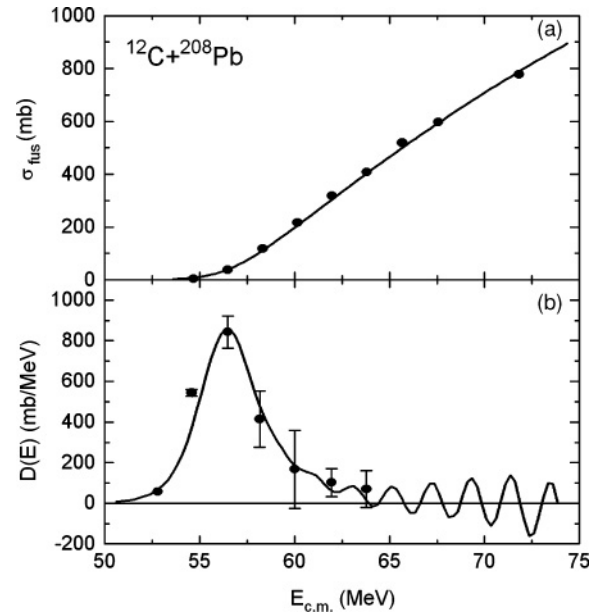


FIG. 5. (a) Variation of fusion cross section σ_{fus} as function of energy $E_{\text{c.m.}}$ for the $^{12}\text{C}+^{208}\text{Pb}$ system. (b) Variation of $D(E_{\text{c.m.}}) = d^2(E_{\text{c.m.}}\sigma_{\text{fus}})/dE_{\text{c.m.}}^2$ as a function of energy $E_{\text{c.m.}}$ corresponding to results of σ_{fus} in upper panel. The full curves represent our calculated results. The experimental data shown by solid dots are obtained from Ref. [3].

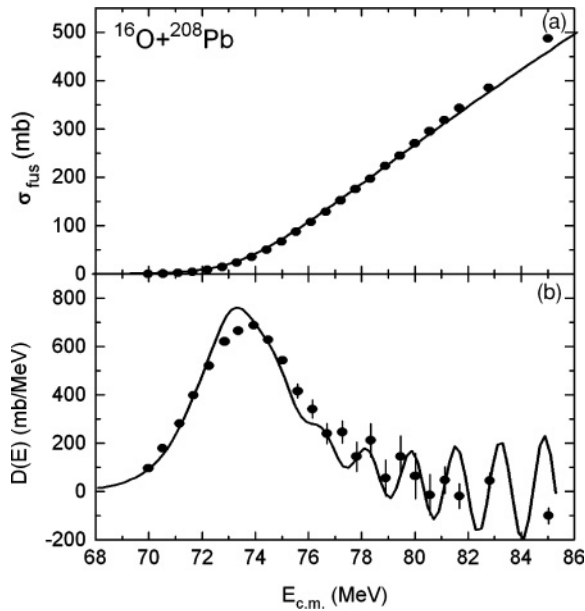


FIG. 6. (a) Variation of σ_{fus} as function of $E_{\text{c.m.}}$ for the $^{16}\text{O}+^{208}\text{Pb}$ system. (b) Variation of $D(E_{\text{c.m.}}) = d^2(E_{\text{c.m.}}\sigma_{\text{fus}})/dE_{\text{c.m.}}^2$ as a function of energy $E_{\text{c.m.}}$ corresponding to results of σ_{fus} in upper panel. The full curves represent our calculated results. The experimental data shown by solid dots are obtained from Ref. [4].

fusion cross sections increases due to the observation [3,19] that there is systematic failure of the Woods-Saxon nuclear potential describing these data, simultaneously.

Similar remarkable success is obtained in the case of the $^{16}\text{O}+^{208}\text{Pb}$ system in matching the experimental data (solid dot) of σ_{fus} taken from Ref. [4] by our calculated results (full curve) shown in Fig. 6(a) over the whole range of energy from $E_{\text{c.m.}} = 68$ to 86 MeV. In this case, the fusion radius used is $R_{\text{fus}} = 8.8$ fm, which is less than the Coulomb radius $R_B = 12.52$ fm. Unlike in the case of $^{12}\text{C}+^{208}\text{Pb}$, in this $^{16}\text{O}+^{208}\text{Pb}$ system, we need to slightly modify the value of the nuclear radius parameter $r_V = 1.35$ fm (see Table I) used in the analysis of scattering data and take $r_V = 1.339$ fm for the fitting of measured σ_{fus} data. However, in both these systems, the values of fusion radius R_{fus} used in our calculation are less than the respective values of Coulomb radius R_B . This clearly demonstrates that fusion is an interior phenomenon, whereas the surface phenomenon is attributed to scattering and other peripheral, less absorptive direct reaction processes. We may mention here that there can be several sets of potential parameters in Woods-Saxon form that give a similar description of elastic-scattering data for a given system. Elastic scattering being a surface phenomenon, it indicates that the height V_B and radial position R_B of the Coulomb barriers produced by all sets of potential parameters are same and fixed, whereas the depth and slope of the effective potential in the interior side $r < R_B$ are different for different sets. However, fusion of two nuclei is an interior phenomenon described by absorption in this region and the corresponding cross section is accounted for by the values of radius parameter R_{fus} that lies in the region $0 < r < R_B$. Depending on the set of potential parameters used in the analysis of scattering, the value of

R_{fus} will be decided and hence it may have different values for different sets of the potential. However, having selected a single potential for the description of both elastic and fusion cross sections, we need not change the value of R_{fus} as a function of energy for the analysis of σ_{fus} at different incident energies. This energy-independent nature of R_{fus} is crucial because it does not complicate the energy derivative of the product $E_{\text{c.m.}}\sigma_{\text{fus}}$ in the results of $d^2(E_{\text{c.m.}}\sigma_{\text{fus}})/dE^2$, which is described in the next subsection. It may be pointed out further that in our calculation, the value of R_{fus} ($=9.9$ fm) in the case of $^{12}\text{C}+^{208}\text{Pb}$ is larger than that (8.8 fm) in the case of $^{16}\text{O}+^{208}\text{Pb}$. This can be ascribed to the fact that with a larger imaginary strength $W = 3.0$ MeV (see Table I) in the case of $^{12}\text{C}+^{208}\text{Pb}$, the corresponding amplitude of the wave function in the interior region is smaller and this requires a larger radius in the summation [Eq. (36)] to account for the experimental data of σ_{fus} . However, with comparatively smaller $W = 2.0$ MeV (see Table I), the amplitude of the wave function is larger and, hence, the value of $R_{\text{fus}} = 8.8$ fm is found to be comparatively less in matching the data in the case of $^{16}\text{O}+^{208}\text{Pb}$. In view of the above fact, we may present the following reason behind the use of large value of $R_{\text{fus}} > R_B$ for a given heavy-ion system in the calculation of Udagawa *et al.* [7]. The magnitude of the imaginary part W of the OMP (see Table I in Ref. [7]) used by this group is very large ($W = 8\text{--}62.9$ MeV) in all the systems stated, in particular it is 22 MeV in the case of $^{16}\text{O}+^{208}\text{Pb}$. This large value of W certainly makes the amplitude of the wave function $\Phi(r)$ negligibly small resulting in a very small value of the product $\text{Im}U(r)|\Phi|^2$ in the interior region and, hence, one has to go beyond R_B to account for the data of σ_{fus} for the given system within the framework of the DRM of fusion.

It may be pointed out here that for the analysis of both elastic and fusion cross sections, we have used smaller values for diffuseness parameter a_V (see Table I) in the OMP of both the systems studied. The resulting sharply falling potential in the interior side of the Coulomb barrier as depicted in Figs. 1 and 3 is found to be crucial in explaining the elastic-scattering cross sections in an energy-independent way. If the value of a_V in a given system is increased to fit the fusion cross-section σ_{fus} data, we have to decrease the value of fusion radius parameter R_{fus} further. However, such a change in a_V disturbs the explanation of elastic-scattering cross sections at various energies presented in Figs. 2 and 4. Hence, for simultaneous fitting of elastic-scattering cross sections and σ_{fus} , we have found a best optimization of the theoretical calculations of these two results at incident energies around the Coulomb barrier. In this calculation, the extraction of σ_{fus} through the method of stepwise absorption with analytical representation is believed to be a unique feature in the analysis of nucleus-nucleus collision process.

We may mention that the use of the shallow imaginary potential in the presence of strong attractive real nuclear potential in our above calculations of cross sections for elastic scattering and fusion gives us some information with regard to structure of the projectile or target nuclei involved in the reaction. The ^{16}O is a doubly magic nucleus having a first excited state 0^+ at 6.049 MeV. ^{12}C also is an even-even nucleus having first excited 2^+ state at 4.4387 MeV. The relatively

small value of strength of the imaginary potential W in our optical potential and the lesser value of $W = 2$ MeV for ^{16}O as compared to $W = 3$ MeV of ^{12}C (see Table I) is consistent with this. In our phenomenological optical potential where the target is also the doubly magic ^{208}Pb , we expect a comparatively lesser role for the excited states of ^{12}C and ^{16}O . However, if a theoretical potential, when ^{12}C or ^{16}O is projectile, is constructed, it will be interesting to see the contribution of low-lying excited states because it is well recognized that some of these states, like the one 0^+ state of ^{12}C at 7.65 MeV, have important significance in nucleosynthesis and astrophysics.

Sometimes, in the optical potential (OP) model description of elastic scattering, both the imaginary and real parts of OP are considered to be depending on the incident energy to account for various reaction channels. The energy dependence of the imaginary potential leads to development of an energy-dependent real potential calculated by using dispersion relation. In our calculation, we are using a very weak imaginary potential. In this case, even if we consider energy dependence in some form, the resulting real part would be weak and this will not affect the results of elastic scattering and fusion as we are using a very strong real part for the nuclear potential.

We may present here the total available experimental results of σ_{fus} (solid dots) from sub-barrier energy to high energy extending up to 90 MeV in the case of $^{12}\text{C}+^{208}\text{Pb}$ in Fig. 7 and up to 109 MeV for $^{16}\text{O}+^{208}\text{Pb}$ in Fig. 8. To explain these results, including high-energy data by our calculated results shown by solid curve in Fig. 7 for the $^{12}\text{C}+^{208}\text{Pb}$ system, we have to use a larger value for Coulomb radius parameter $r_C = 1.4$ fm instead of $r_C = 0.9$ fm used earlier for results of σ_{fus} at low energy shown in Fig. 5(a) by solid curve. Similarly, we use $r_C = 1.37$ fm instead of $r_C = 1.02$ fm to calculate results of σ_{fus} (solid curve) to fit the high-energy data for the $^{16}\text{O}+^{208}\text{Pb}$ reaction in Fig. 8. We may mention that this need to change r_C to larger value to fit the higher energy data is equivalent to incorporating indirectly the energy dependence for the total potential. However, in our present calculation,

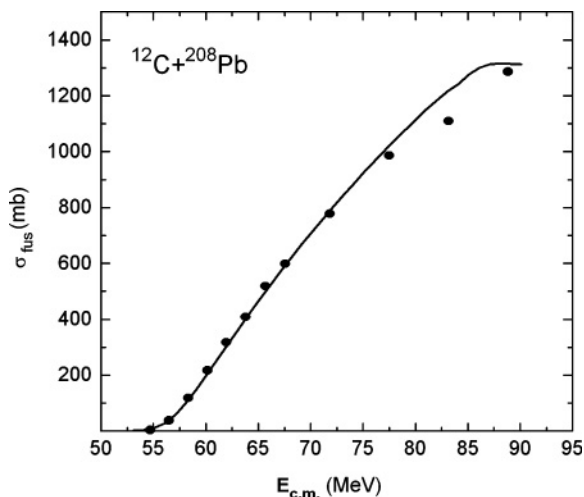


FIG. 7. Variation of fusion cross section σ_{fus} as function of energy $E_{\text{c.m.}}$ for the $^{12}\text{C}+^{208}\text{Pb}$ system. The full curve represents our calculated results with $r_C = 1.4$ fm. The experimental data shown by solid dots are obtained from Ref. [3].

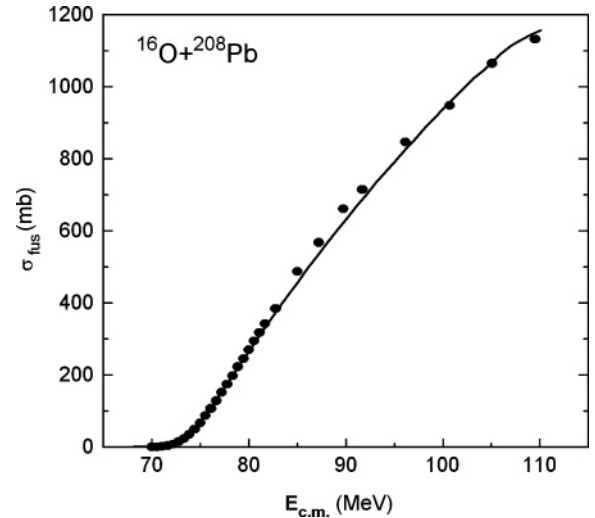


FIG. 8. Same as Fig. 7 for for the $^{16}\text{O}+^{208}\text{Pb}$ system. The full curve represents our calculated results with $r_C = 1.37$ fm. The experimental data shown by solid dots are obtained from Ref. [4].

we focus on the unified description of an elastic-scattering cross section, σ_{fus} and results of $D(E_{\text{c.m.}}) = d^2(E\sigma_{\text{fus}})/dE^2$ in the low-energy region covering near and sub-barrier energy around the Coulomb barrier. In this region of energy, the process of fusion of two heavy nuclei is believed to be the prominent reaction channel and other reaction channels, if present, are considered weak and peripheral. This allows one to consider an energy-independent potential to study scattering and accompanying fusion in this low energy. The energy-independent optical potential found for the successful analysis of elastic scattering will help us in explaining the peak structure of the quantity $D(E_{\text{c.m.}}) = d^2(E\sigma_{\text{fus}})/dE^2$, which does not allow any extra energy dependence of σ_{fus} in its process of derivation or formulation through the optical potential and regionwise absorption.

C. Explanation of $D(E_{\text{c.m.}})$

The above results of σ_{fus} both from experiment and theory as a function of energy as presented in Figs. 5(a) and 6(a) do not show any kind of structure. Hence, from this fitting of the monotonically varying data, nothing more can be said about the possible physical phenomena that might be playing some role in the fusion process. To get some insight into these processes, the same results of σ_{fus} is presented in a different form as follows. One can extract values of a quantity that is the second derivative of the product $E_{\text{c.m.}}\sigma_{\text{fus}}$ denoted by $D(E_{\text{c.m.}}) = d^2(E_{\text{c.m.}}\sigma_{\text{fus}})/dE_{\text{c.m.}}^2$ with respect to energy $E_{\text{c.m.}}$. For this, the following point difference formula can be used:

$$D(E) = [(E - \Delta E)\sigma_- - 2E\sigma + (E + \Delta E)\sigma_+]/(\Delta E)^2, \quad (37)$$

where σ_- , σ , and σ_+ indicate fusion cross sections σ_{fus} at center-of-mass energies $E - \Delta E$, E and $E + \Delta E$, respectively, with energy step size ΔE . Function $D(E_{\text{c.m.}})$ is generally referred to as barrier distribution [5,33,34]. By using

formula (37), the extracted results obtained from the measured values of σ_{fus} as a function of energy for the $^{12}\text{C}+^{208}\text{Pb}$ system are obtained from Ref. [3] and are shown in Fig. 5(b) as solid dots for analysis. The same results of $^{16}\text{O}+^{208}\text{Pb}$ obtained from Ref. [4] are shown in Fig. 6(b) as solid dots. The data in the latter system in Fig. 6(b) show large oscillation as compared to the former in Fig. 5(b). We now explain these experimental results by our calculation.

Using the same formula (37), we obtain the results of the quantity $D(E_{c.m.})$ as a function of $E_{c.m.}$ from our calculated results of σ_{fus} . In Fig. 5(b), we show our results by solid curve and compare them with the corresponding experimental data (solid dots) for the $^{12}\text{C}+^{208}\text{Pb}$ system. It is seen that the main peak along with some smaller peaks in the higher energy region are well reproduced by our calculation. Similarly, in Fig. 6(b), we obtain remarkable matching of the highly oscillatory structure of the measured data of $D(E_{c.m.})$ in the case of the $^{16}\text{O}+^{208}\text{Pb}$ system. More importantly the negative nature of some of the dips in the higher-energy region are accounted for quite well. The importance of this successful explanation increases due to the observation [4] that the more microscopic coupled-channels calculation [35] for fusion has failed to explain the data of $D(E_{c.m.})$ in the $^{16}\text{O}+^{208}\text{Pb}$ system [4,16]. We may point out here that the above oscillatory structure both in $^{12}\text{C}+^{208}\text{Pb}$ and $^{16}\text{O}+^{208}\text{Pb}$ systems can be destroyed by three ways: (i) by increasing the strength of imaginary part W , (ii) by considering a larger value for the Coulomb radius parameter r_C , and (iii) by increasing the step size ΔE for differentiation through formula (37). The values of W and r_C are fixed looking to the accurate explanation of the elastic-scattering data along with the explanation of measured results of σ_{fus} and $D(E_{c.m.})$. As recorded in Table I, the value of W is 3 MeV for $^{12}\text{C}+^{208}\text{Pb}$ and 2 MeV for $^{16}\text{O}+^{208}\text{Pb}$. The value of r_C is taken to be $r_C = 0.9$ fm for $^{12}\text{C}+^{208}\text{Pb}$ and $r_C = 1.02$ fm for $^{16}\text{O}+^{208}\text{Pb}$ to fit the measured data of $D(E_{c.m.})$ well along with the σ_{fus} data in Figs. 5(a) and 6(a), respectively, in the lower-energy region around the Coulomb barrier where the results of $D(E_{c.m.})$ are reported prominently by experiments.

Having obtained this remarkable fitting of the peculiar peak structure of the measured data of the quantity $D(E_{c.m.}) = d^2(E_{c.m.}\sigma_{\text{fus}})/dE_{c.m.}^2$, we theorize the presence of the following physical phenomenon that might be giving rise to such structure in the process of fusion of the two heavy nuclei.

An ion-ion effective potential that possesses a deep pocket followed by a thick barrier in a given partial wave trajectory can support wave functions with the proper number of radial nodes giving rise to discrete resonance states called shape resonances that may not be observed experimentally [6]. In the potential scattering theory, these resonances are manifested clearly as maxima in the results of reaction cross section (σ_r) at the respective resonance energies [36]. The interior pocket of the effective potential is further controlled by the Coulomb radius parameter r_C . Smaller value of r_C makes the pocket ‘‘U’’ type that generates more oscillation in σ_r to manifest resonances. The width of a resonance so generated by the real part of the potential increases if the potential is made more absorptive using larger imaginary part W . Consequently, larger width leads to extinction of the corresponding resonance in the

collision process. In our analysis of $^{12}\text{C}+^{208}\text{Pb}$ and $^{16}\text{O}+^{208}\text{Pb}$ collisions, we have considered a deep real potential associated with a relatively weak imaginary strength W . This potential can generate many resonances that can be clearly visible in the form of peaks in the variation of partial wave reaction cross section as a function of energy in different partial wave (ℓ) trajectories. Each partial wave gives rise to resonance structure. It is the cumulative effect of all these resonance structures that is primarily responsible for the oscillation in $D(E_{c.m.})$. This is confirmed by noting that if W is increased, resonance structures in different ℓ s and the oscillations in $D(E_{c.m.})$ vanish. Because precise experimental data of resonances for $^{12}\text{C}+^{208}\text{Pb}$ and $^{16}\text{O}+^{208}\text{Pb}$ systems are not available we refrain from listing the energies of these resonances. Nevertheless, based on our present calculation and also Ref. [37], we believe that oscillations in $D(E_{c.m.})$ are indicator of critical role played by the heavy-ion resonances in fusion cross sections. With this it may be conjectured that the process of fusion of two nuclei at low energy can be understood as an event passing through the formation of compound nucleus that is represented by shape resonances and, hence, these resonances might be acting as doorway states for the fusion process.

IV. SUMMARY AND CONCLUSION

The Schroedinger equation with composite optical potential of two interacting nuclei is solved analytically to give an expression for the scattering matrix with a recursive mathematical structure. Using the same potential and the wave function, an analytical formula for absorption cross section is derived to account for the reaction cross section. The formulation is applied to the $^{12}\text{C}+^{208}\text{Pb}$ and $^{16}\text{O}+^{208}\text{Pb}$ systems for the analysis of the following experimental data in a consistent manner.

- (i) The angular variation of differential scattering cross section at several energies around the Coulomb barrier.
- (ii) Fusion cross-section σ_{fus} as function of energy over a wide range covering the Coulomb barrier region.
- (iii) The extracted result of the quantity $D(E_{c.m.}) = d^2(E_{c.m.}\sigma_{\text{fus}})/dE_{c.m.}^2$.

The important features that emerge from this analysis can be summarized as follows:

- (a) A single but complex nuclear potential in Woods-Saxon form without any energy dependence is found to be successful in explaining the elastic-scattering data at several energies. Large depth and small diffuseness in the real part and weak strength (less absorption) in the imaginary part are important features of the complex optical potential used in the calculation.
- (b) Estimation of the part of reaction cross section to account for the fusion cross section through the method of stepwise absorption is a significant feature in the calculation. This process of partitioning the total reaction cross section is natural in the sense that we never use any extra energy dependence in the process of extraction nor the imaginary part is partitioned arbitrarily.

- (c) The results of σ_{fus} presented in another form, namely $D(E_{\text{c.m.}}) = d^2(E_{\text{c.m.}}\sigma_{\text{fus}})/dE_{\text{c.m.}}^2$ by using point difference formula show peculiar peak structure in its variation with $E_{\text{c.m.}}$. This result with peaks and dips is explained with remarkable success by our calculated results of σ_{fus} expressed in the above form.
- (d) The weakly absorptive nature of the optical potential mentioned in item (a) above is found to allow resonance states to occur in the collision of the two

nuclei. These resonances are then found to control the oscillatory or peak structure of $D(E_{\text{c.m.}})$ stated in point (c) above.

ACKNOWLEDGMENTS

This work was supported by the Department of Science and Technology (DST), New Delhi, India vide Research Grant no. SR/S2/HEP-18/2004.

-
- [1] S. Santra, P. Singh, S. Kailas, A. Chatterjee, A. Shrivastava, and K. Mahata, *Phys. Rev. C* **64**, 024602 (2001).
- [2] F. Videbaek, R. B. Goldstein, L. Grodzins, S. G. Steadman, T. A. Belote, and J. D. Garrett, *Phys. Rev. C* **15**, 954 (1977).
- [3] A. Mukherjee, D. J. Hinde, M. Dasgupta, K. Hagino, J. O. Newton, and R. D. Butt, *Phys. Rev. C* **75**, 044608 (2007).
- [4] C. R. Morton, A. C. Berriman, M. Dasgupta, D. J. Hinde, J. O. Newton, K. Hagino, and I. J. Thompson, *Phys. Rev. C* **60**, 044608 (1999).
- [5] M. Dasgupta, D. J. Hinde, N. Rowley, and A. M. Stefanini, *Annu. Rev. Nucl. Part. Sci.* **48**, 401 (1998), and references therein.
- [6] Y. Eisen and Z. Vager, *Nucl. Phys.* **A187**, 219 (1972).
- [7] T. Udagawa, B. T. Kim, and T. Tamura, *Phys. Rev. C* **32**, 124 (1985).
- [8] T. Udagawa, S.-W. Hong, and T. Tamura, *Phys. Rev. C* **32**, 1435 (1985).
- [9] J. R. Birkelund and J. R. Huizenga, *Annu. Rev. Nucl. Part. Sci.* **33**, 265 (1983).
- [10] S. G. Steadman and M. J. Rhoades-Brown, *Annu. Rev. Nucl. Part. Sci.* **36**, 649 (1986).
- [11] G. R. Satchler, M. A. Nagarajan, J. S. Lilley, and I. J. Thompson, *Phys. Rev. C* **41**, 1869 (1990).
- [12] M. A. Nagarajan and G. R. Satchler, *Phys. Lett.* **B173**, 29 (1986).
- [13] C. H. Dasso and S. Landowne, *Comput. Phys. Commun.* **46**, 187 (1987); M. Dasgupta, A. Navin, Y. K. Agrawal, C. V. K. Baba, H. C. Jain, M. L. Thingan, and A. Roy, *Nucl. Phys.* **A539**, 351 (1992).
- [14] I. J. Thompson, *Comput. Phys. Rep.* **7**, 167 (1998).
- [15] K. Hagino, N. Rowley, and A. T. Kruppa, *Comput. Phys. Commun.* **123**, 143 (1999).
- [16] H. Esbensen and S. Misiu, *Phys. Rev. C* **76**, 054609 (2007).
- [17] M. Dasgupta, D. J. Hinde, A. Diaz-Torres, B. Bouriquet, C. I. Low, G. J. Milburn, and J. O. Newton, *Phys. Rev. Lett.* **99**, 192701 (2007).
- [18] R. N. Sagaidak, S. P. Tretyakova, S. V. Khlebnikov, A. A. Ogloblin, N. Rowley, and W. H. Trzaska, *Phys. Rev. C* **76**, 034605 (2007).
- [19] J. O. Newton, R. D. Butt, M. Dasgupta, D. J. Hinde, I. I. Gontchar, C. R. Morton, and K. Hagino, *Phys. Rev. C* **70**, 024605 (2004).
- [20] D. J. Hinde, M. Dasgupta, C. R. Morton, A. C. Berriman, R. D. Butt, and J. O. Newton, *Nucl. Phys.* **A654**, 864c (1999); D. J. Hinde, C. R. Morton, M. Dasgupta, J. R. Leigh, J. C. Mein, and H. Timmers, *Nucl. Phys.* **A592**, 271 (1995).
- [21] M. R. Spinella, J. E. Testoni, O. Dragun, and H. D. Matra, *Nucl. Phys.* **A687**, 385 (2001).
- [22] G. R. Satchler, M. A. Nagarajan, J. S. Lilley, and I. J. Thompson, *Ann. Phys.* **178**, 110 (1987).
- [23] M. L. Halbert, J. R. Beene, D. C. Hensley, K. Honkanen, T. M. Semkow, V. Abenante, D. G. Sarantites, and Z. Li, *Phys. Rev. C* **40**, 2558 (1989).
- [24] R. H. Landau and M. J. P. Mejia A, *Computational Physics Problem Solving with Computers* (John Wiley & Sons Inc., New York, 1997).
- [25] F. R. Loscalzo and T. D. Talbot, *Bull. Amer. Math. Soc.* **73**, 438 (1967).
- [26] G. Micula, *Math. Comp.* **27**, 807 (1973).
- [27] B. Sahu, B. B. Sahu, and S. K. Agarwalla, *Pram. J. Phys.* **70**, 27 (2008).
- [28] M. A. Melkanoff, J. Raynal, and T. Sawada, *Methods in Computational Physics, Vol. VI* (Academic Press, New York, 1966).
- [29] C. S. Shastri and Y. K. Gambhir, *Phys. Rev. C* **28**, 1109 (1983).
- [30] M. P. Nicoli, F. Haas, R. M. Freeman, N. Aissaoui, C. Beck, A. Elanique, R. Nouicer, A. Morsad, S. Szilner, Z. Basrak, M. E. Brandan, and G. R. Satchler, *Phys. Rev. C* **60**, 064608 (1999).
- [31] S. C. Pieper, M. J. Rhoades-Brown, and S. Landowne, *Phys. Lett.* **B162**, 43 (1985).
- [32] R. M. Devries and M. R. Clover, *Nucl. Phys.* **A243**, 528 (1975).
- [33] A. B. Balantekin and N. Takigawa, *Rev. Mod. Phys.* **70**, 77 (1998).
- [34] J. R. Leigh, M. Dasgupta, D. J. Hinde, J. C. Mein, C. R. Morton, R. C. Lemmon, J. P. Lestone, J. O. Newton, H. Timmers, J. X. Wei, and N. Rowley, *Phys. Rev. C* **52**, 3151 (1995).
- [35] N. Rowley, G. R. Satchler, and P. H. Stelson, *Phys. Lett.* **B254**, 25 (1991).
- [36] B. Sahu, L. Satpathy, and C. S. Shastri, *Phys. Lett.* **A303**, 105 (2002).
- [37] B. Sahu, S. K. Agarwalla, and C. S. Shastri, *Nucl. Phys.* **A713**, 45 (2003).